Mitochondrial Ca^{2+} Uptake Correlates with the Severity of the Symptoms in Autosomal Dominant Optic Atrophy

László Fülöp[a], Anikó Rajki[b], Erika Maka[c], Mária Judit Molnár[d], András Spät[a*]

Departments of [a]Physiology, [c]Ophthalmology and [d] Genomic Medicine and Rare Diseases, Semmelweis University Medical School, Budapest, Hungary and [b]Laboratory of Molecular Physiology, Hungarian Academy of Sciences, Budapest, Hungary

[*]Corresponding author: Department of Physiology, Semmelweis University Medical School, P.O.B. 259, H-1444 Budapest, Hungary
e-mail: spat@eok.sote.hu, phone: +36 1 459-1500 ext. 60427, fax: + 36 1 266 7480

Keywords: optic atrophy, fibroblast, OPA1, calcium ion, mitochondria, apoptosis, ganglion cell

ABSTRACT

The most frequent form of hereditary blindness, Autosomal Dominant Optic Atrophy (ADOA) is caused by the mutation of the mitochondrial protein Opa1 and the ensuing degeneration of retinal ganglion cells. Previously we found that knockdown of *OPA1* enhanced mitochondrial Ca^{2+} uptake (Fülöp *et al.*,PLoS One 2011). Therefore we studied mitochondrial Ca^{2+} metabolism in fibroblasts obtained from members of an ADOA family. Gene sequencing revealed heterozygosity for a splice site mutation (c. 984+1G>A) in intron 9 of the *OPA1* gene. ADOA cells showed a higher rate of apoptosis than control cells and their mitochondria displayed increased fragmentation when forced to oxidative metabolism. The ophthalmological parameters critical fusion frequency and ganglion cell – inner plexiform layer thickness were inversely correlated to the evoked mitochondrial Ca^{2+} signals. The present data indicate that enhanced mitochondrial Ca^{2+} uptake is a pathogenetic factor in the progress of ADOA.

1. Introduction

The most frequent form of hereditary blindness is autosomal dominant optic atrophy (ADOA, OMIM165500). The disorder is due to cell death confined to retinal ganglion cells which results in bilateral central visual loss, impaired color vision and central visual field defects [1,2]. The prevalence of ADOA is estimated to be between 1/50,000 and 1/10,000 [3,4]. The most frequent cause of type 1 ADOA is the mutation of the *OPA1* gene [5–7]. Opa1 is a dynamin-related GTPase protein and due to alternative splicing its gene is transcribed into 8 mRNA isoforms in human [7] encoding proteins of 924-1014 amino acids. The protein is tethered to the IMM [8–10] and localized in the IMS [8,9]. In Western blot analysis 5 separate bands (designated *a* to *e*) ranging from 94 to 86 kDa, can be detected. Two long isoforms are anchored to the IMM and three soluble short forms are located in the IMS. The soluble forms are the proteolytic products of the long isoforms [11,12]. (For further details see recently publised excellent reviews [13,14].)

The fundamental pathology in ADOA is the degeneration of the small (parvo) retinal ganglion cells with subsequent atrophy of the optic nerve [13,15,16]. Nevertheless, the protein is expressed in all examined human tissues, explaining the accidental development of the so-called 'ADOA +' forms characterized by the association of the blindness with various neuromuscular disorders [17–19] or hearing loss [20,21]. The vulnerability of retinal ganglion cells and that of spiral ganglion cells in the inner ear [22] has been attributed to the impairment of ATP production as observed in fibroblasts [23,24] or skeletal muscle [25]. Since retinal ganglion cells are unique among neurons in that the are exposed to direct sunlight, the ensuing oxidative stress may potentiate the consequences of Opa1 dysfunction, leading to apoptosis of these cells [13]. In *OPA1*$^{+/-}$ mice the level of postsynaptic density protein 95 and the density of glutamatergic synaptic sites were reduced even without loss of mitochondrial membrane potential [26]. This observation indicates the significance of Opa1 in maintaining the synaptic architecture and connectivity of retinal ganglion cells.

Knockdown of *OPA1* in two human cell lines, in HeLa and H295R (adrenocortical) cells, induces enhanced mitochondrial Ca^{2+} uptake [27] and also mitochondrial Ca^{2+} -dependent hypersecretion of aldosterone (in H295R cells) [28]. On the other hand, excessive accumulation of Ca^{2+} by mitochondria leads to cell death [29–31]. In view of these observations it was reasonable to examine mitochondrial Ca^{2+} uptake in ADOA patients. Our present data showed a correlation between the Ca^{2+} sequestring ability of mitochondria and the grade of impairment of visual parameters.

2. Materials and Methods

2.1 Materials

Bradykinin and digitonin were purchased from Sigma-Aldrich (St. Louis, MO, USA). Silencing RNA products, Rhod-2 AM, Fluo-4 AM, Mito Tracker Deep Red (MTDR), tetramethylrhodamine ethyl ester (TMRE) and 5,5′,6,6′-tetrachloro-1,1′,3,3′-tetraethyl-

imidacarbocyanine iodide (JC-1) were purchased from Life Technologies (Paisley, UK). Annexin V-FITC was from BD Biosciences, glucose-free medium (E15-079) was from GE Healthcare (Piscataway, NJ). D-galactose was purchased from Reanal (Budapest, Hungary). Fetal bovine serum (FBS) was obtained from Lonza (Basel, Switzerland). Antibodies were used as follows: anti-OPA1 mouse monoclonal antibody (612606, BD Biosciences), anti-protein disulphide isomerase mouse monoclonal antibody (ab2792, Abcam, Cambridge, UK), anti-mouse immunoglobulin-HRP (NA 931V, GE Healthcare).

2.2 Clinical studies

Seven members of a family with genetically verified ADOA were subjected to detailed ophthalmological and neurological examinations including the tests for far and near visual acuity (spec. No. 2305 and 2307) (logarithmic visual acuity chart, from Precision Vision, Artesia LA), measurement of thickness of retinal nerve fibre layer, ganglion cell and inner plexiform layer (optical coherence tomography, Cirrhus HD-OCT, Carl Zeiss Meditec, Dublin LA) and critical flicker fusion frequency (CFF). Written informed consent was obtained from all patients and controls. As control, two healthy volunteers were also examined. After obtaining appropriate consent skin samples used for fibroblast culturing were excised from all five adult subjects. The reserach was approved by Hungarian Research Ethical Committee and carried out according to the Helsinki declaration.

2.3 Gene sequencing

Sequencing of the coding region and the exon-intron junctions of the *OPA1* gene (NM 015560.2) in patient I/3 was performed by Dr. Josseline Kaplan at the Service Medicale, GH Necker Enf. Malades, F-75743 Paris Cedex 15, France. Subsequently the segregation analysis of the mutation in the affected family members was performed in our laboratory using ABI Prism 3500 DNA Sequencer (Applied Biosystems, Foster City, CA). Genetic sequence was compared with the human reference genome (NM_001005360, ENSG00000079805) using NCBI's Blast® application.

2.4 Cell culture and transfection

Fibroblasts acquired from human skin biopsies were grown in DMEM containing 20% heat inactivated FBS, 100 U/ml penicillin and 100 µg/ml streptomycin. Passage numbers 3 -7 were used.

2.5 Apoptosis

Control cells or cells exposed to 0.1 mM H_2O_2 for 4 hours at 37^oC were dyed with FITC labeled annexin V (1:100) in a binding buffer (10 mM HEPES pH 7.4, 140 mM NaCl, 2.5 mM $CaCl_2$) for 15 minutes. The cells were examined with confocal microscopy.

2.6 Experimental conditions

The cells were superfused at room temperature with a modified Krebs-Ringer solution containing 140 mM Na^+, 4.5 mM K^+, 1.2 mM Ca^{2+}, 0.5 mM Mg^{2+}, 5 mM Hepes and 2 mM HCO_3^- (pH 7.4). Flow rate was ~1ml/min. Permeabilization with 25 μM digitonin (for 8 min) was carried out in a cytosol-like medium (117 mM KCl, 6 mM NaCl, 1 mM KH_2PO_4, 2 mM Na^+ pyruvate, 2 mM Na^+ succinate, 2 mM K^+ ADP, 2 mM EGTA, 0.5 mM Mg^{2+} and 10 mM K^+ HEPES). The medium containing 5 μM free Ca^{2+} was composed with the Chelator software [32].

2.7 Confocal microscopy

Cytoplasmic and mitochondrial Ca^{2+} uptake (monitored with Fluo-4 and Rhod-2, resp.), mitochondrial membrane potential (TMRE or JC-1) and mitochondrial morphology (MTDR) were examined with confocal microscopy (LSM 510) as described [27]. Apoptosis was studied applying annexin V-FITC with a Zeiss LSM 710 confocal laser scanning microscope, equipped with a 63x/1.4 oil immersion objective (Plan-Apochromat, Zeiss) and operated with ZEN 9.0 software.

2.8 Electrophoresis and immunoblotting

SDS electrophoresis and immunoblotting were performed as described [27]. Anti-Opa1 and anti-PDI primary antibodies and anti-mouse secondary antibody were applied at a dilution of 1:500, 1:3000 and 1:5000, respectively. Protein content of the samples was measured with BCA assay.

2.9 Statistics

Means $\pm$ S.E.M. are shown. For estimating significance of differences Kruskal-Wallis test (followed by Dunnett's test) was used. Correlation was calculated with Pearson's or Spearman's test. Data were analyzed with Statistica 11.

3. Results

3.1 Clinical examinations and genetic analysis

Seven members of a family with hereditary visual impairment were subjected to detailed ophthalmological and neurological examination (Fig 1a, Table 1 and Suppl. Tables 1 – 5). The most severe progress of ADOA has been diagnosed in patient I/1. Patient I/1 and I/2 beside the visual impairment, had mild neurological symptoms. The four children did not have any neurological symptoms. We had no contact with the mother of the three adult siblings but based on the hetero-anamnestic data, she had serious visual impairment. The diagnosis has been confirmed in all the seven patients by genetic investigations which revealed a new heterozygous splice site mutation (c. 984+1G>A) in the *OPA1* gene. Western blot analysis of fibroblasts from patient I/1 detected reduced expression of Opa1 (as related to protein disulphide isomerase), however, there was no change in the pattern of OPA1 isoforms (Fig. 1b). The results of the Western blot are

compatible with the ability of the antibody to recognize amino acids 708-830, a site downstream of the splice site mutation.

For studying mitochondrial state and function, fibroblasts were cultured from the three adult patients (I/1, I/2 and I/3) who also showed mild neurological symptoms (Suppl. Tables 3-5) and two healthy controls (Ctrl2 and Ctrl2). In these five subjects strong correlation was found between the functional parameter CFF and the thickness of retinal gangion cell - inner plexiform layer ($R^2 = 0.961$, $p = 0.0197$) (Suppl. Fig. 1).

3.2 Morphology of mitochondria

Morphology of mitochondria in fibroblasts of the most severely diseased patient I/1 (Table 1) was examined with MTDR staining. No difference could be observed between control and ADOA samples under control conditions. When oxidative (mitochondrial) metabolism was forced by culturing the cells in galactose containing medium for 72 hours [23] significant mitochondrial fragmentation took place in the mutant cells whereas the effect was negligible in the controls (Suppl. Figs 2 - 4).

3.3 Mitochondrial Ca^{2+} uptake

In order to elucidate whether mutant fibroblast cells have enhanced mitochondrial Ca^{2+} uptake as observed in *Opa1* silenced human cell lines [27] we monitored cytosolic and mitochondrial [Ca^{2+}] with Fluo-4 and Rhod-2, respectively. Stimulation with 1 nM bradykinin evoked a rapid cytosolic Ca^{2+} signal that was ensued by a more prolonged increase in mitochondrial [Ca^{2+}] (Figs 2a, c and d). Since mitochondrial Ca^{2+} uptake depends on the amplitude of cytosolic Ca^{2+} signal, the mitochondrial responses were also related to the cytosolic responses (Fig. 2e). The peak of mitochondrial Ca^{2+} signal exceeded that of the pooled controls only in the cells of patient I/1 ($p = 0.015$) who, out of the 3 siblings, displayed the greatest progress of ADOA. Mitochondrial membrane potential in her fibroblasts, measured with TMRE and JC-1, was comparable with that of controls (not shown), therefore no change in the driving force could account for the enhanced mitochondrial Ca^{2+} uptake.

To rule out any cytosolic factor modifying mitochondrial Ca^{2+} metabolism, the transport was examined also in permeabilized cells. Replacing the Ca^{2+} free cytosol-like superfusion medium with one containing 5 μM Ca^{2+} induced a rapid increase in mitochondrial [Ca^{2+}] (Fig. 2b). Both the slope and the peak of mitochondrial Ca^{2+} signal in the fibroblasts of patient I/1 exceeded those of controls ($p = 0.007$ and 0.015, resp., Fig. 2f), ruling out the role of cytosolic factors in the enhancement of mitochondrial Ca^{2+} sequestring ability.

3.4 Apoptosis

Deficient Opa1 function enhances apoptotic processes both under control conditions and after exposure to apoptotic stimuli. It may have diagnostic significance that progression of ADOA is indicated by increased apoptosis rate [13]. Therefore we examined the apoptotic state of the cultured fibroblasts with FITC-labelled annexin V. This fluorescent ligand attaches to the cell membrane already in an early stage of the

apoptosis. Under resting conditions the apoptotic rate was already higher in the ADOA patients (15 % vs. 2.5 % in average, Fig. 3c). Four hours after exposing the fibroblasts to the apoptotic reagent H_2O_2 (0.1 mM) the apoptotic rate in the ADOA cells (27 % in average) far exceeded that in the controls (5.3 %) (Fig. 3d and Suppl. Fig. 5). These observations show increased sensitivity of ADOA cells to apoptotic stimuli.

3.5 Clinical data in function of mitochondrial Ca^{2+}

The purpose of the present study was to elucidate the role of mitochondrial Ca^{2+} in the development of visual impairment in ADOA patients. Therefore we analyzed the correlation between the peak of bradykinin-induced mitochondrial Ca^{2+} uptake and the clinical parameters in all five examined subjects. A significant correlation was found between $[Ca^{2+}]_m$ and CFF ($p=0.0232$, Fig. 3a) as well as $[Ca^{2+}]_m$ and the thickness of ganglion cell layer ($p=0.0283$, Fig. 3b) of these patients. Very high apoptosis rate was observed in resting (Fig. 3c) and H_2O_2 - stimulated cells (Fig. 3d) of patient I/1 who showed the highest Ca^{2+} response to bradykinin. At the same time, the fibroblasts of patient I/3 displayed moderate ophthalmological alterations despite displaying control-like mitochondrial Ca^{2+} parameters. This latter observation indicates that retinal damage may begin before any detectable change in cellular Ca^{2+} metabolism occurs.

4. Discussion

Opa1 regulates mitochondrial morphology [33]. Knockdown of the *OPA1* gene brings about the fragmentation of mitochondria [10,34,35] and drastic desorganisation of the cristae [34,36–39]. Also, Opa1 defect often leads to apoptosis [34,40].

The majority of cytochrome *c* reductase and F_1F_0 ATPase [41], that of cytochrome *c* oxidase [42] as well as the uncoupling protein 1 (in brown adipocytes) [43] are found within the crista membrane. Only 10-15 % of cytochrome *c* is found free in the intermembrane space while the major fraction can be found in the cristae [44,45]. The release of cytochrome *c* from digitonin-permeabilized mitochondria is significantly enhanced after exposure to t-Bid that evokes the disassembly of Opa1 oligomers [40,46] and a drastic increase in the junction diameter (i.e. the transition between the so-called inner boundary membrane and crista membrane) [45]. These data indicate that diffusion through the junction is controlled by Opa1. Dilatation of the junction may facilitate the diffusion between the intermembrane space and the lumen of cristae and thus may modify mitochondrial metabolism [13,47].

In the fibroblasts of ADOA patients mutations in the GTPase domain or deletion of the GTPase effector domain increased the susceptibility to apoptosis, irrespective of whether mitochondria were fragmented or not [48]. Cell death may be a consequence of excessive Ca^{2+} loading of mitochondria [29–31]. Yet, we are not aware of studies on mitochondrial Ca^{2+} metabolism in ADOA patients. Therefore we studied mitochondrial Ca^{2+} uptake in ADOA patients, using their cultured fibroblasts under well-controlled laboratory conditons.

Ca^{2+} uptake from the mitochondrial intermembrane space into the mitochondrial matrix occurs predominantly through the MCU complex containing the Ca^{2+} selective ion channel MCU (*Mitochondrial Calcium Uniporter)* [49,50] and several accessory

proteins [51–54]. Recalling that *OPA1* knockdown increases the diffusibility of cytochrome *c* through the crista junctions [38,45,46] we postulated that if significant Ca^{2+} uptake into the matrix occurs from the lumen of the cristae, reduced expression of Opa1 would increase the access of Ca^{2+} to the transporters in the crista membrane and consequently would enhance Ca^{2+} uptake. Experimental results have supported this postulation. In HeLa and H295R adrenocortical cells agonist-induced cytosolic Ca^{2+} signals were transferred into the mitochondria. The rate and amplitude of the secondary mitochondrial [Ca^{2+}] rise were increased after knockdown of *OPA1*, as compared with cells transfected with control RNA or *mitofusin1* siRNA. (*Mfn1* siRNA was applied as control for *OPA1* siRNA since they induced comparable fragmentation of the mitochondrial network.) In permeabilized cells the rate of Ca^{2+} uptake by depolarized mitochondria was also increased in *OPA1*-silenced cells. The enhancement of Ca^{2+} transport seemed to be independent of Mitochondrial Permeability Transition Pore, since it was not influenced by its inhibitor cyclosporin A [27]. The biological significance of the enhanced Ca^{2+} uptake in OPA1-silenced H295R cells was indicated by enhanced aldosterone production [28]. Although our data in HeLa cells were partly at variance with those of Kushnareva *et al.* [55] (in this respect see [56]), studies on the Ca^{2+} retention capacity of mitochondria in *OPA1*-silenced murine retinal ganglion cells [16] and the Ca^{2+} sensitivity of mitochondrial permeability transition pore in *OPA1*-silenced HeLa cells [55] are in harmony with our observations. The report that knock-down of *Opa1* increased the amplitude of Ca^{2+} uptake and the Ca^{2+} retention capacity in murine cardiac mitochondria [57] also supports the conclusion that an impairment of OPA1 function may lead to enhanced mitochondrial Ca^{2+} signalling.

The alteration of Ca^{2+} metabolism in *OPA1*-silenced cells led to the idea that enhanced mitochondrial Ca^{2+} uptake in ADOA patients may be a factor participating in the pathogenesis of blindness. In this respect it has no significance whether the increase of mitochondrial Ca^{2+} uptake was induced solely by enhanced diffusion of Ca^{2+} to MCU within the cristae or also alteration in the expression profile or location of mitochondrial Ca^{2+} handling proteins. In the family investigated in this study three generations of patients showed the dominant nature of their visual impairment. Sequence analysis of *OPA1* gene detected a previously non-described mutation (c. 984+1G>A) in intron 9. The Western blot analysis of the fibroblasts revealed reduced expression of Opa1 protein but no detectable change in the isoform pattern. In fact, no change in the ratio of long and short isoforms are expected in case of mutation at the splice site of the 9th intron since alternate splicings (yielding short isoforms) are evoked by cleavage in exons 4, 4b or 5b [13,58]. The applied antibody recognizes amino acids 708-830 therefore it may not recognize any mutant protein.

Based on the severity of their complains, their visual acuity, thickness of the retinal ganglion cell layer and CFF patient I/1 showed the most progressed stage of ADOA. All the examined adult patients exhibited slight neurological symptoms as well, therefore the disease of this family may be regarded as "ADOA +". Their mitochondrial morphology was comparable to that of the two control subjects when the fibroblasts were cultured under conventional conditions., However, when fibroblasts were forced to rely on oxidative (mitochondria – dependent) metabolism by the application of a galactose-containing medium [23] striking mitochondrial fragmentation took place. This observation revealed the incipient impairment of mitochondrial function.

The present study revealed a significant negative correlation between mitochondrial Ca^{2+} uptake and two clinically important ophthalmological parameters, namely CFF and the thickness of the retinal ganglion cell – inner plexiform layer. Now the question may arise what the causal relation between Ca^{2+} uptake and retinal damage is. The bulk of evidence shows that excessive Ca^{2+} uptake may lead to cell death. On the other hand, moderate impairment of several ophthalmological parameters could already be measured in patient I/3, although her Ca^{2+} parameters were comparable with those of the controls. As far as conclusion may be drawn at the low number of observations the present data suggest that retinal damage may begin without a detectable change in mitochondrial Ca^{2+} uptake whereas further enhancement of Ca^{2+} uptake contributes to the progress of the disease. However, if mitochondrial turnover rate is higher in the retinal ganglion cells than in fibroblasts depletion of the normal Opa1 pool might occur earlier in the ganglion cells than in fibroblasts and in such a case a causative role of Ca^{2+} in triggering ADOA cannot be ruled out.

Acknowledgements

The present study has been supported by the Hungarian Academy of Sciences and the Hungarian Brain Research Program (KTIA 13 NAP-A-III/6). The skilful technical help of med. stud. Katalin Kelényi is appreciated.

References

1. M.Votruba, Molecular genetic basis of primary inherited optic neuropathies, Eye (Lond) 18 (2004) 1126-1132.

2. M.V.Alavi, N.Fuhrmann, Dominant optic atrophy, OPA1, and mitochondrial quality control: understanding mitochondrial network dynamics, Mol Neurodegener 8 (2013) 32-42.

3. B.Kjer, H.Eiberg, P.Kjer, T.Rosenberg, Dominant optic atrophy mapped to chromosome 3q region. II. Clinical and epidemiological aspects, Acta Ophthalmol Scand 74 (1996) 3-7.

4. A.Russo, L.Delcassi, E.Marchina, F.Semeraro, Correlation between visual acuity and OCT-measured retinal nerve fiber layer thickness in a family with ADOA and an OPA1 mutation, Ophthalmic Genet 34 (2013) 69-74.

5. C.Alexander, M.Votruba, U.E.Pesch, D.L.Thiselton, S.Mayer, A.Moore, M.Rodriguez, U.Kellner, B.Leo-Kottler, G.Auburger, S.S.Bhattacharya, B.Wissinger, OPA1, encoding a dynamin-related GTPase, is mutated in autosomal dominant optic atrophy linked to chromosome 3q28, Nat Genet 26 (2000) 211-215.

6. C.Delettre, G.Lenaers, J.M.Griffoin, N.Gigarel, C.Lorenzo, P.Belenguer, L.Pelloquin, J.Grosgeorge, C.Turc-Carel, E.Perret, C.Astarie-Dequeker, L.Lasquellec, B.Arnaud, B.Ducommun, J.Kaplan, C.P.Hamel, Nuclear gene OPA1, encoding a mitochondrial dynamin-related protein, is mutated in dominant optic atrophy, Nat Genet 26 (2000) 207-210.

7. C.Delettre, J.M.Griffoin, J.Kaplan, H.Dollfus, B.Lorenz, L.Faivre, G.Lenaers, P.Belenguer, C.P.Hamel, Mutation spectrum and splicing variants in the OPA1 gene, Hum Genet 109 (2001) 584-591.

8. E.D.Wong, J.A.Wagner, S.W.Gorsich, J.M.McCaffery, J.M.Shaw, J.Nunnari, The dynamin-related GTPase, Mgm1p, is an intermembrane space protein required for maintenance of fusion competent mitochondria, J Cell Biol 151 (2000) 341-352.

9. M.Satoh, T.Hamamoto, N.Seo, Y.Kagawa, H.Endo, Differential sublocalization of the dynamin-related protein OPA1 isoforms in mitochondria, Biochemical and Biophysical Research Communications 300 (2003) 482-493.

10. L.Griparic, N.N.van der Wel, I.J.Orozco, P.J.Peters, A.M.van der Bliek, Loss of the intermembrane space protein Mgm1/OPA1 induces swelling and localized constrictions along the lengths of mitochondria, Journal of Biological Chemistry 279 (2004) 18792-18798.

11. N.Ishihara, Y.Fujita, T.Oka, K.Mihara, Regulation of mitochondrial morphology through proteolytic cleavage of OPA1, EMBO Journal 25 (2006) 2966-2977.

12. L.Griparic, T.Kanazawa, A.M.van der Bliek, Regulation of the mitochondrial dynamin-like protein Opa1 by proteolytic cleavage, Journal of Cell Biology 178 (2007) 757-764.

13. G.Lenaers, P.Reynier, G.Elachouri, C.Soukkarieh, A.Olichon, P.Belenguer, L.Baricault, B.Ducommun, C.Hamel, C.Delettre, OPA1 functions in mitochondria and dysfunctions in optic nerve, Int J Biochem Cell Biol 41 (2009) 1866-1874.

14. P.Belenguer, L.Pellegrini, The dynamin GTPase OPA1: More than mitochondria?, Biochim Biophys Acta 1833 (2013) 176-183.

15. M.Liesa, M.Palacin, A.Zorzano, Mitochondrial dynamics in mammalian health and disease, Physiological Reviews 89 (2009) 799-845.

16. G.Dayanithi, M.Chen-Kuo-Chang, C.Viero, C.Hamel, A.Muller, G.Lenaers, Characterization of Ca^{2+} signalling in postnatal mouse retinal ganglion cells: involvement of OPA1 in Ca^{2+} clearance, Ophthalmic Genet 31 (2010) 53-65.

17. G.Hudson, P.Amati-Bonneau, E.L.Blakely, J.D.Stewart, L.He, A.M.Schaefer, P.G.Griffiths, K.Ahlqvist, A.Suomalainen, P.Reynier, R.McFarland, D.M.Turnbull, P.F.Chinnery, R.W.Taylor, Mutation of OPA1 causes dominant optic atrophy with external ophthalmoplegia, ataxia, deafness and multiple mitochondrial DNA deletions: a novel disorder of mtDNA maintenance, Brain 131 (2008) 329-337.

18. P.Yu-Wai-Man, K.S.Sitarz, D.C.Samuels, P.G.Griffiths, A.K.Reeve, L.A.Bindoff, R.Horvath, P.F.Chinnery, OPA1 mutations cause cytochrome c oxidase deficiency due to loss of wild-type mtDNA molecules, Hum Mol Genet 19 (2010) 3043-3052.

19. C.P.Schaaf, M.Blazo, R.A.Lewis, R.E.Tonini, H.Takei, J.Wang, L.J.Wong, F.Scaglia, Early-onset severe neuromuscular phenotype associated with compound heterozygosity for OPA1 mutations, Mol Genet Metab 103 (2011) 383-387.

20. P.Amati-Bonneau, A.Guichet, A.Olichon, A.Chevrollier, F.Viala, S.Miot, C.Ayuso, S.Odent, C.Arrouet, C.Verny, M.N.Calmels, G.Simard, P.Belenguer, J.Wang, J.L.Puel, C.Hamel, Y.Malthiery, D.Bonneau, G.Lenaers, P.Reynier, OPA1 R445H mutation in optic atrophy associated with sensorineural deafness, Ann Neurol 58 (2005) 958-963.

21. S.Leruez, D.Milea, S.Defoort-Dhellemmes, E.Colin, M.Crochet, V.Procaccio, M.Ferre, J.Lamblin, V.Drouin, C.Vincent-Delorme, G.Lenaers, C.Hamel, C.Blanchet, G.Juul, M.Larsen, C.Verny, P.Reynier, P.Amati-Bonneau, D.Bonneau, Sensorineural hearing loss in OPA1-linked disorders, Brain 136 (2013) e236.

22. S.Bette, U.Zimmermann, B.Wissinger, M.Knipper, OPA1, the disease gene for optic atrophy type Kjer, is expressed in the inner ear, Histochem Cell Biol 128 (2007) 421-430.

23. C.Zanna, A.Ghelli, A.M.Porcelli, M.Karbowski, R.J.Youle, S.Schimpf, B.Wissinger, M.Pinti, A.Cossarizza, S.Vidoni, M.L.Valentino, M.Rugolo, V.Carelli, OPA1 mutations associated with dominant optic atrophy impair oxidative phosphorylation and mitochondrial fusion, Brain 131 (2008) 352-367.

24. A.Chevrollier, V.Guillet, D.Loiseau, N.Gueguen, M.A.de Crescenzo, C.Verny, M.Ferre, H.Dollfus, S.Odent, D.Milea, C.Goizet, P.Amati-Bonneau, V.Procaccio, D.Bonneau, P.Reynier, Hereditary optic neuropathies share a common mitochondrial coupling defect 2, Ann Neurol 63 (2008) 794-798.

25. R.Lodi, C.Tonon, M.Valentino, D.Manners, C.Testa, E.Malucelli, C.La Morgia, P.Barboni, M.Carbonelli, S.Schimpf, B.Wissinger, M.Zeviani, A.Baruzzi, R.Liguori, B.Barbiroli, V.Carelli, Defective mitochondrial adenosine triphosphate production in skeletal muscle from patients with dominant optic atrophy due to OPA1 mutations, Arch Neurol 68 (2012) 67-73.

26. P.A.Williams, M.Piechota, R.C.von, E.Taylor, J.E.Morgan, M.Votruba, Opa1 is essential for retinal ganglion cell synaptic architecture and connectivity, Brain 135 (2012) 493-505.

27. L.Fülöp, G.Szanda, B.Enyedi, P.Várnai, A.Spät, The effect of OPA1 on mitochondrial Ca^{2+} signaling, PLoS One 6 (2011) e25199.

28. A.Spät, L.Fülöp, G.Szanda, The role of mitochondrial Ca^{2+} and NAD(P)H in the control of aldosterone secretion, Cell Calcium 52 (2012) 64-72.

29. M.Zoratti, I.Szabo, The mitochondrial permeability transition, Biochim Biophys Acta 1241 (1995) 139-176.

30. P.Bernardi, A.Rasola, Calcium and cell death: the mitochondrial connection, Subcell Biochem 45 (2007) 481-506.

31. M.R.Duchen, Mitochondria and Ca^{2+} in cell physiology and pathophysiology, Cell Calcium 28 (2000) 339-348.

32. T.J.Schoenmakers, G.J.Visser, G.Flik, A.P.Theuvenet, CHELATOR: an improved method for computing metal ion concentrations in physiological solutions, Biotechniques 12 (1992) 870-876.

33. C.S.Palmer, L.D.Osellame, D.Stojanovski, M.T.Ryan, The regulation of mitochondrial morphology: intricate mechanisms and dynamic machinery, Cell Signal 23 (2011) 1534-1545.

34. A.Olichon, L.Baricault, N.Gas, E.Guillou, A.Valette, P.Belenguer, G.Lenaers, Loss of OPA1 perturbates the mitochondrial inner membrane structure and integrity, leading to cytochrome c release and apoptosis, Journal of Biological Chemistry 278 (2003) 7743-7746.

35. S.Cipolat, d.B.Martins, B.Dal Zilio, L.Scorrano, OPA1 requires mitofusin 1 to promote mitochondrial fusion, Proc Natl Acad Sci U S A 101 (2004) 15927-15932.

36. H.Sesaki, S.M.Southard, M.P.Yaffe, R.E.Jensen, Mgm1p, a dynamin-related GTPase, is essential for fusion of the mitochondrial outer membrane, Mol Biol Cell 14 (2003) 2342-2356.

37. B.Amutha, D.M.Gordon, Y.Gu, D.Pain, A novel role of Mgm1p, a dynamin-related GTPase, in ATP synthase assembly and cristae formation/maintenance, Biochem J 381 (2004) 19-23.

38. D.Arnoult, A.Grodet, Y.J.Lee, J.Estaquier, C.Blackstone, Release of OPA1 during apoptosis participates in the rapid and complete release of cytochrome c and subsequent mitochondrial fragmentation, Journal of Biological Chemistry 280 (2005) 35742-35750.

39. C.Merkwirth, S.Dargazanli, T.Tatsuta, S.Geimer, B.Lower, F.T.Wunderlich, J.C.Kleist-Retzow, A.Waisman, B.Westermann, T.Langer, Prohibitins control cell proliferation and apoptosis by regulating OPA1-dependent cristae morphogenesis in mitochondria, Genes Dev 22 (2008) 476-488.

40. C.Frezza, S.Cipolat, d.B.Martins, M.Micaroni, G.V.Beznoussenko, T.Rudka, D.Bartoli, R.S.Polishuck, N.N.Danial, B.De Strooper, L.Scorrano, OPA1 controls apoptotic cristae remodeling independently from mitochondrial fusion, Cell 126 (2006) 177-189.

41. R.W.Gilkerson, J.M.Selker, R.A.Capaldi, The cristal membrane of mitochondria is the principal site of oxidative phosphorylation, FEBS Letters 546 (2003) 355-358.

42. M.E.Perotti, W.A.Anderson, H.Swift, Quantitative cytochemistry of the diaminobenzidine cytochrome oxidase reaction product in mitochondria of cardiac muscle and pancreas, J Histochem Cytochem 31 (1983) 351-365.

43. D.Loncar, Immunoelectron microscopical studies on synthesis and localization of uncoupling protein in brown adipocytes: evidence for cotranslational transport of uncoupling protein into mitochondria, J Struct Biol 105 (1990) 133-145.

44. P.Bernardi, G.F.Azzone, Cytochrome c as an electron shuttle between the outer and inner mitochondrial membranes, Journal of Biological Chemistry 256 (1981) 7187-7192.

45. L.Scorrano, M.Ashiya, K.Buttle, S.Weiler, S.A.Oakes, C.A.Mannella, S.J.Korsmeyer, A distinct pathway remodels mitochondrial cristae and mobilizes cytochrome c during apoptosis, Dev Cell 2 (2002) 55-67.

46. R.Yamaguchi, L.Lartigue, G.Perkins, R.T.Scott, A.Dixit, Y.Kushnareva, T.Kuwana, M.H.Ellisman, D.D.Newmeyer, Opa1-mediated cristae opening is Bax/Bak and BH3 dependent, required for apoptosis, and independent of Bak oligomerization, Mol Cell 31 (2008) 557-569.

47. T.G.Frey, C.W.Renken, G.A.Perkins, Insight into mitochondrial structure and function from electron tomography, Biochim Biophys Acta 1555 (2002) 196-203.

48. A.Olichon, T.Landes, L.Arnaune-Pelloquin, L.J.Emorine, V.Mils, A.Guichet, C.Delettre, C.Hamel, P.Amati-Bonneau, D.Bonneau, P.Reynier, G.Lenaers,

P.Belenguer, Effects of OPA1 mutations on mitochondrial morphology and apoptosis: relevance to ADOA pathogenesis, J Cell Physiol 211 (2007) 423-430.

49. J.M.Baughman, F.Perocchi, H.S.Girgis, M.Plovanich, C.A.Belcher-Timme, Y.Sancak, X.R.Bao, L.Strittmatter, O.Goldberger, R.L.Bogorad, V.Koteliansky, V.K.Mootha, Integrative genomics identifies MCU as an essential component of the mitochondrial calcium uniporter, Nature 476 (2011) 341-345.

50. D.De Stefani, A.Raffaello, E.Teardo, I.Szabo, R.Rizzuto, A forty-kilodalton protein of the inner membrane is the mitochondrial calcium uniporter, Nature 476 (2011) 336-340.

51. S.Marchi, P.Pinton, The mitochondrial calcium uniporter complex: molecular components, structure and physiopathological implications, J Physiol 592 (2014) 829-839.

52. M.Patron, A.Raffaello, V.Granatiero, A.Tosatto, G.Merli, S.D.De, L.Wright, G.Pallafacchina, A.Terrin, C.Mammucari, R.Rizzuto, The Mitochondrial Calcium Uniporter (MCU): molecular identity and physiological roles, J Biol Chem 288 (2013) 10750-10758.

53. D.Pendin, E.Greotti, T.Pozzan, The elusive importance of being a mitochondrial Ca uniporter, Cell Calcium 55 (2014) 139-145.

54. N.E.Hoffman, H.C.Chandramoorthy, S.Shanmughapriya, X.Q.Zhang, S.Vallem, P.J.Doonan, K.Malliankaraman, S.Guo, S.Rajan, J.W.Elrod, W.J.Koch, J.Y.Cheung,

M.Madesh, SLC25A23 augments mitochondrial Ca^{2+} uptake, interacts with MCU, and induces oxidative stress-mediated cell death, Mol Biol Cell 25 (2014) 936-947.

55. Y.E.Kushnareva, A.A.Gerencser, B.Bossy, W.K.Ju, A.D.White, J.Waggoner, M.H.Ellisman, G.Perkins, E.Bossy-Wetzel, Loss of OPA1 disturbs cellular calcium homeostasis and sensitizes for excitotoxicity, Cell Death Differ 20 (2012) 353-365.

56. L.Fülöp, A.Rajki, D.Katona, G.Szanda, A.Spät, Extramitochondrial OPA1 and adrenocortical function, Mol Cell Endocrinol 381 (2013) 70-79.

57. J.Piquereau, F.Caffin, M.Novotova, A.Prola, A.Garnier, P.Mateo, D.Fortin, L.H.Huynh, V.Nicolas, M.Alavi, C.Brenner, R.Ventura-Clapier, V.Veksler, F.Joubert, Downregulation of OPA1 alters mouse mitochondrial morphology, PTP function, and cardiac adaptation to pressure overload, Cardiovasc Res 94 (2012) 408-417.

58. Z.Song, H.Chen, M.Fiket, C.Alexander, D.C.Chan, OPA1 processing controls mitochondrial fusion and is regulated by mRNA splicing, membrane potential, and Yme1L, Journal of Cell Biology 178 (2007) 749-755.

Legend of Figures

Fig. 1. Mutation *OPA1* gene and reduced expression of intact Opa1 protein. (**A**) Genealogical tree of the examined ADOA family. The filled-in symbols represent carriers of a splice site mutation (c. 984+1G>A) in intron 9 of the *OPA1* gene. The arrow shows the proband (the first affected family member who sought medical attention for her genetic disorder). (**B**) Western blot revealed reduced protein expression but maintained ratio of *L* (long) and *S* (short) isoforms in patient I/1 as compared to the control person Ctrl1. (NB The applied anti-Opa1 antibody does not recognize the mutated protein.) Protein disulphide isomerase (PDI) was used as loading control.

Fig. 2. Mitochondrial Ca^{2+} uptake. (**A**) Bradykinin (1 nM) - induced Ca^{2+} signal as monitored with laser scanning confocal microscopy in an intact control cell. The cell was preloaded with Fluo-4 and Rhod-2 for monitoring changes of cytosolic and mitochondrial [Ca^{2+}], respectively. Stimulation is indicated by horizontal line. (**B**) Mitochondrial Ca^{2+} signal (Ca^{2+}_m) in a permeabilized, Rhod-2 preloaded cell. Ca^{2+} uptake was induced by replacing the Ca^{2+} -free cytosol-like superfusion medium with one containing 5 μM Ca^{2+}, as indicated by horizontal line. (**C**) The peak of bradykinin - induced cytosolic Ca^{2+} signal, related to Fluo-4 fluorescence in the control period, is shown. (**D**) The peak of bradykinin - induced mitochondrial Ca^{2+} signal, related to Rhod-2 fluorescence in the control period, is shown. (**E**) The peak of bradykinin - induced mitochondrial Ca^{2+} signal related to the corresponding cytosolic Ca^{2+} peak (Ca^{2+}_m/Ca^{2+}_c) is shown. (**F**) The initial rate of mitochondrial Ca^{2+} uptake ($\Delta Ca^{2+}_m/\Delta t$, blue) and maximal mitochondrial Ca^{2+} uptake (yellow) in permeabilized cells after raising the [Ca^{2+}] of the Ca^{2+} -free cytosol-like superfusion medium with one containing 5 μM Ca^{2+}. In panels C-E the number of cells is shown in the bottom of the respective columns.

Fig. 3. Correlation between the ratio of mitochondrial to cytosolic Ca^{2+} signals (mean $\pm$ S.E.M., see Fig. 2E) and (**A**) Critical Fusion Frequency (CFF, see Table 1), (**B**) thickness of ganglion cell and inner plexifrom layer (see Table 1) and (**C**) percentage of apoptotic fibroblasts incubated without or (**D**) after 4 hr exposure to 0.1 mM H_2O_2 . Control data are shown in white, ADOA data are shown in red. The number of examined cells was between 60 and 300 per subject.

A

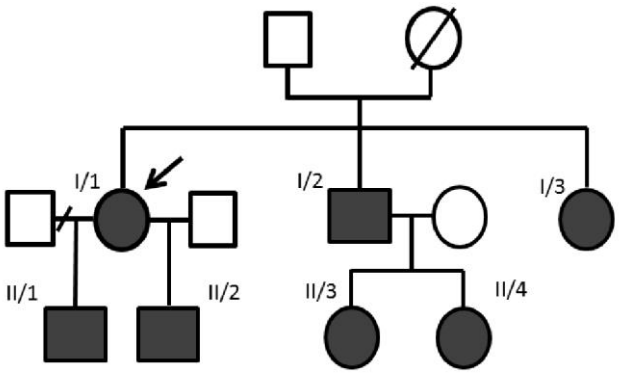
I/1
I/2
I/3
II/1
II/2
II/3
II/4

B

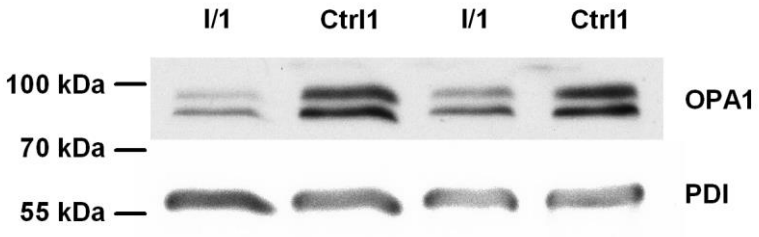
I/1
Ctrl1
I/1
Ctrl1
100 kDa
70 kDa
55 kDa
OPA1
PDI

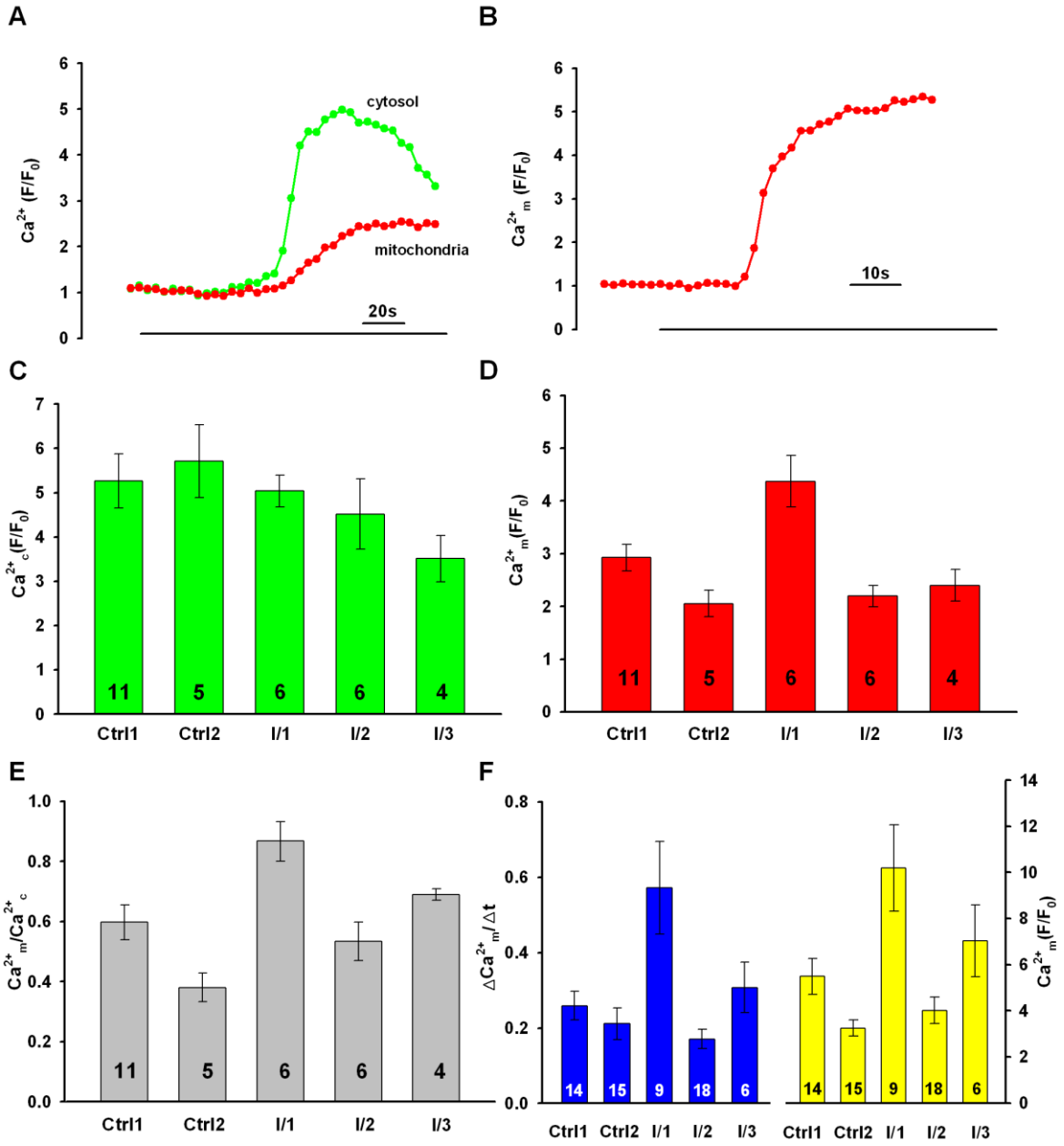
A
B
C
D
E
F
cytosol
mitochondria
20s
10s
Ctrl1
Ctrl2
I/1
I/2
I/3
11
5
6
6
4
14
15
9
18
6

Table 1 Ophthalmological data of the examined subjects

name	gender	age (year)	visual acuity (far, right)	mean RNFL thickness (right)	mean ganglion cell + IPL thickness (right)	CFF (Hz), right	CFF (Hz), left
I/1	F	38	0.16	59 (1)	42 (1)	32	32
I/2	M	43	0.1	59 (1)	49 (1)	34	34
I/3	F	36	0.16	61 (1)	55 (1)	36	36
II/1	M	11	0.25				
II/2	M	6	0.1				
II/3	F	6	0.5				
II/4	F	8	0.32			38	38
Ctrl1	M	28	1.6	88 (22)	86 (59)	40	40
Ctrl2	M	35	1.25	98 (65)	80 (26)	40	40

RNFL retinal nerve fiber layer, *IPL* inner plexiform layer, *CFF* critical flicker fusion frequency

Normal range for visual acuity is ≥1; that for CFF is ≥40. Thickness is expressed in μm, the values in brackets show the percentile values of age-matched controls.

Legend of suppl. Figures

Suppl. Fig.1**.** Correlation of critical flicker fusion frequency (CFF) and mean thickness of retinal gangion cell - inner plexiform layer (IPL) ($R^2 = 0.961$, $p = 0.0197$). The patients' data are shown with dark circle, the pooled control data are shown with empty circles.

Suppl. Fig.2**.** Examples for (**A**) filamentous, (**B**) balloon-like and (**C**) fragmented mitochondrial pattern. The optical slice was 1.1 μM.

Suppl. Fig.3. Morphology of mitochondria derived from (**A**) control Ctrl1 and (**B**) patient I/1, after incubating the fibroblasts for 72 hours in galactose-containing medium. The optical slice was 1.1 μM.

Suppl. Fig. 4. Mitochondrial morphology. Morphology of mitochondria as classified by Zanna *et al.* [23], is shown after incubation in control (glucose containing) medium or after 4 days incubation in galactose containing medium. Forty cells of control Ctrl1 and 31 cells of patient I/1 were examined after culturing in control medium whereas 27 and 36 cells, resp., were studied after incubation in galactose containing medium. For images of filamentous, balloon-like and fragmented mitochondria see Suppl. Fig. 1.

Suppl. Fig. 5. Examination of apoptosis in fibroblasts of (**A**) control Ctrl1 and (**B**) patient I/1 after 4 hr exposure to 0.1 μM H_2O_2. The cells were dyed with Annexin V – FITC. The optical slice was 2.5 μM.

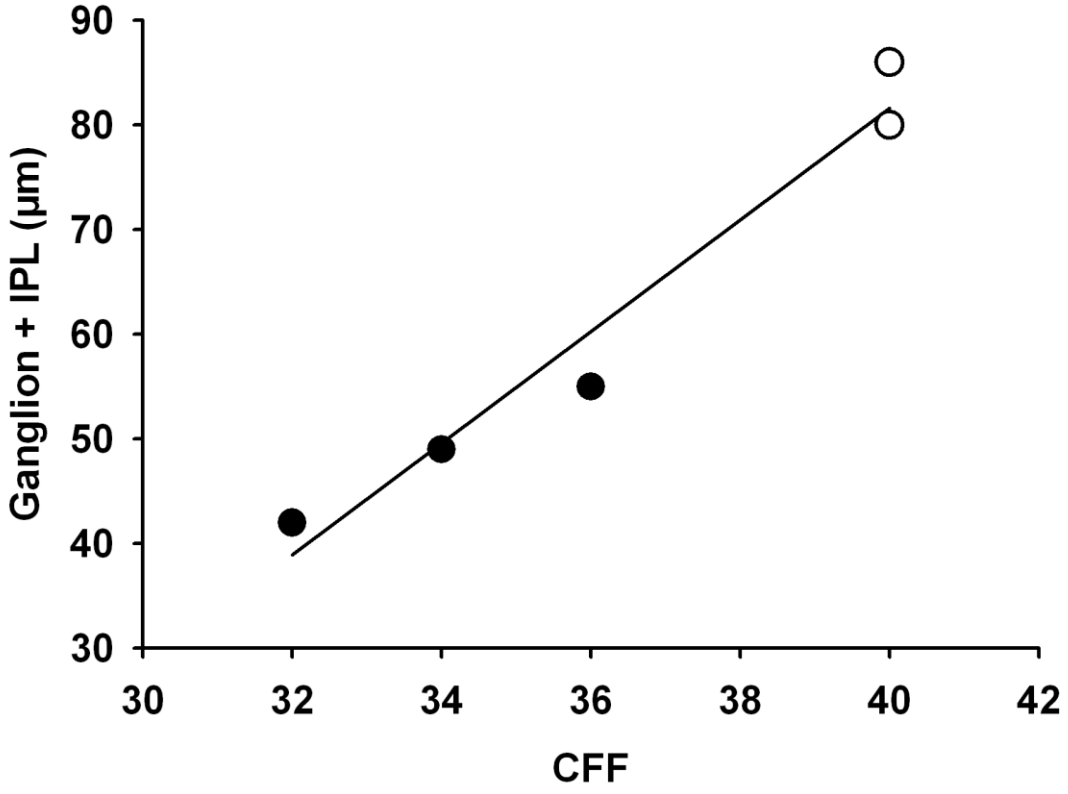
90
80
70
60
50
40
30
Ganglion + IPL (µm)
30
32
34
36
38
40
42
CFF

A

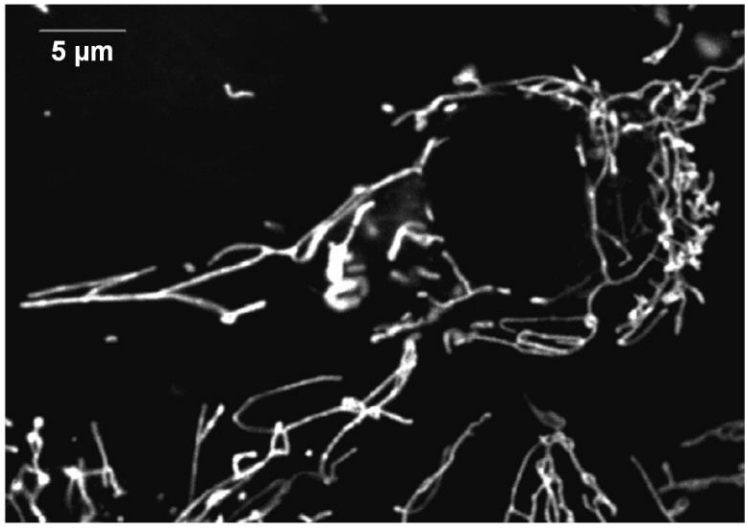

B

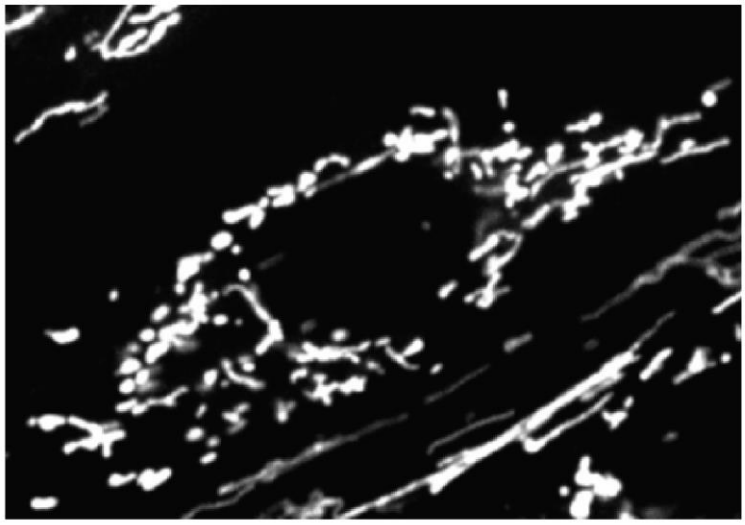

C

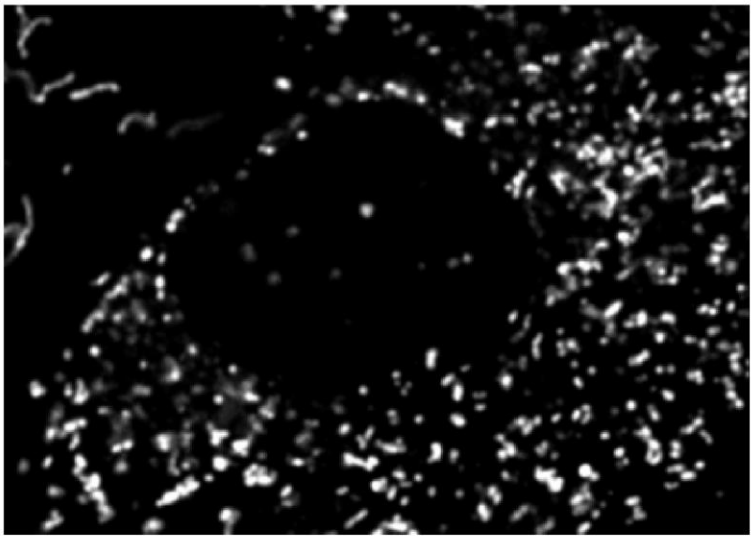

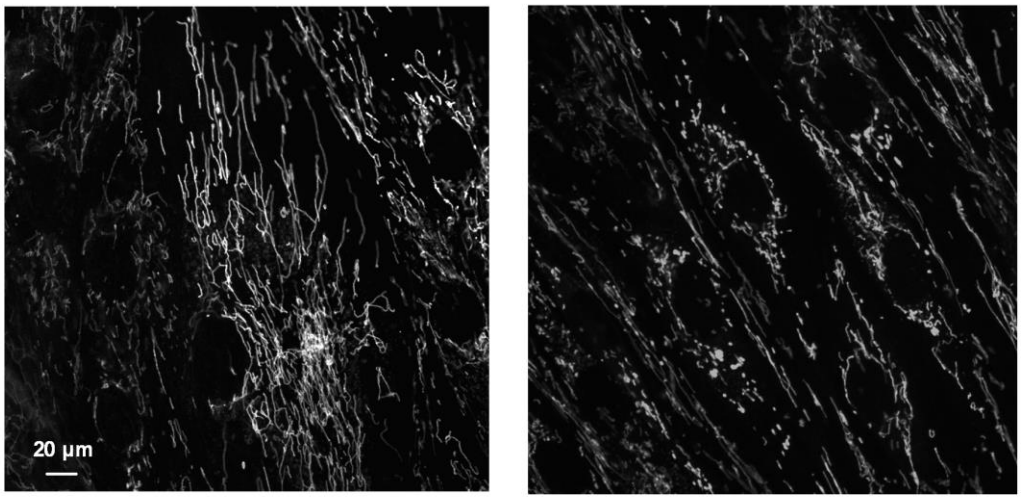

Ctrl1 I/1

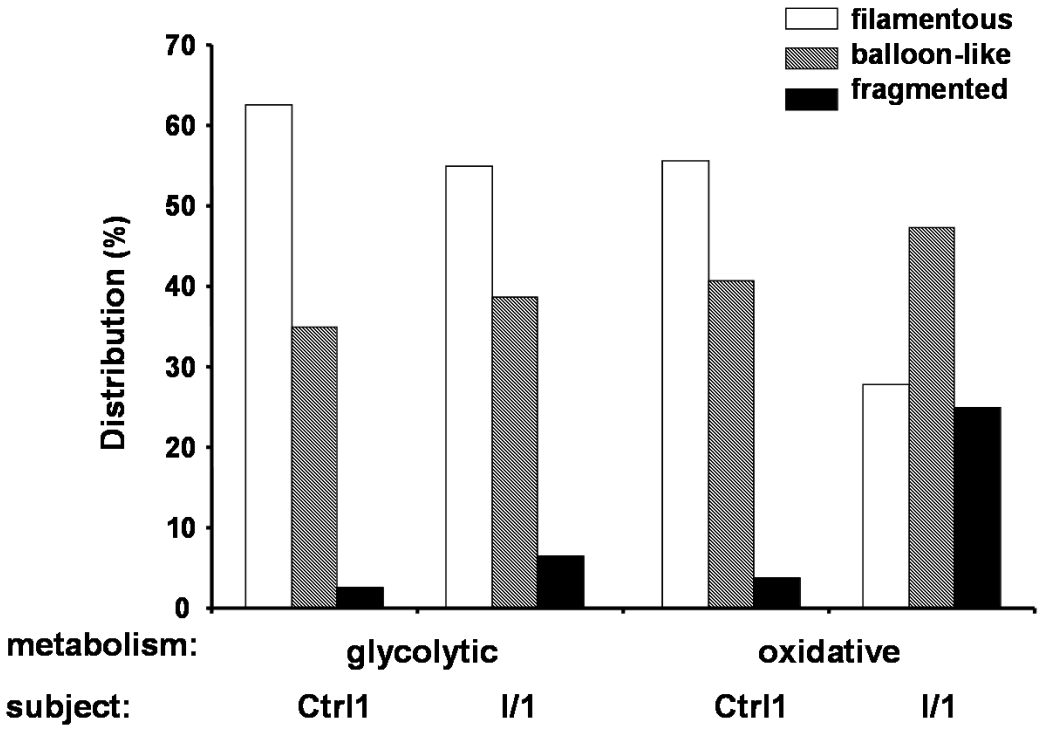
filamentous
balloon-like
fragmented
Distribution (%)
70
60
50
40
30
20
10
0
metabolism:
glycolytic
oxidative
subject:
Ctrl1
I/1
Ctrl1
I/1

Supplementary Table 1 Results of ophthalmological examinations*

name	gender	Visual acquity far, right	Visual acuity far, left	Visual acuity near, right	Visual acuity near, left	mean ganglion cell + IPL thickness right	mean ganglion cell + IPL thickness left	CFF (Hz), right	CFF (Hz), left
I/1	F	0.16	0.1	0.25	0.2	42 (1)	42 (1)	32	32
I/2	M	0.1	0.063	0.16	0.1	49 (1)	50 (1)	34	34
I/3	F	0.16	0.125	0.08	0.1	55 (1)	52 (1)	36	36
Ctrl1	M	1.6	1.6	1	1	86 (59)	85 (53)	40	40
Ctrl2	M	1.25	1.25	1	1	80 (26)	77 (15)	40	40

*Thickness is expressed in µm, the values in brackets show the percentile values of age-matched controls

RNFL retinal nerve fiber layer, *IPL* inner plexiform layer, *CFF* critical flicker fusion frequency

Normal range for visual acuity is ≥1; that for CFF is ≥40

Supplementary Table 2 Results of ophthalmological examinations: thickness* of retinal nerve fibre layer (RNFL)

Name	RNFL right superior	RNFL right nasal	RNFL right inferior	RNFL right temporal	RNFL left superior	RNFL left nasal	RNFL left inferior	RNFL left temporal
I/1	62 (1)	63 (29)	69 (1)	41 (1)	78 (1)	61 (22)	86 (1)	41 (1)
I/2	70 (1)	55 (7)	63 (1)	49 (5)	82 (1)	56 (13)	64 (1)	46 (3)
I/3	71 (1)	54 (9)	69 (1)	48 (7)	69 (1)	56 (11)	68 (1)	35 (1)
Ctrl1	121 (48)	62 (22)	113 (19)	57 (21)	126 (62)	59 (17)	104 (6)	63 (43)
Ctrl2	116 (41)	70 (49)	138 (82)	67 (63)	108 (22)	57 (13)	108 (15)	81 (90)

*Thickness is expressed in µm, the values in brackets show the percentile values of age-matched controls.

Supplementary Table 3 The neurological symptoms of Patients I/1, I/2 and I/3

Patient	**Hypoacusis**	**Paresis**	**Deep tendon reflexes**	**Ataxia**	**Peripheral sensory deficit**
I/1	No	No	Decreased in the upper limbs	Dysmetria and mild limb ataxia in the upper limbs	No
I/2	Yes	No	Decreased in all 4 limbs	Dysmetria and mild limb ataxia in the upper limbs	No
I/3	No	No	Normal	Mild dysmetria in the upper limbs	No

Supplementary Table 4 VEP component latency in full field stimulation of Patients I/1, I/2, I/3

Patient	VEP Studies					
	Left Eye (Cz-Oz)			Right Eye (Cz-Oz)		
	N75 (ms)	P100.(ms)	N145 (ms)	N70 (ms)	P100.(ms)	N145 (ms)
I/1	U	U	U	U	U	U
I/2	U	U	U	U	U	U
I/3	91.5	129.8	165.3	91.8	124.5	160.5

N and P: positive (P) or negative (N) wave, the following number indicates the average peak latency

U: unreproducible

Supplementary Table 5 Nerve conduction studies

Patient	Left median nerve motor			Left peroneal nerve motor			Right sural nerve		
	DL (ms)	Ampl (mV)	CV (m/s)	DL (ms)	Ampl (mV)	CV (m/s)	DL (ms)	Ampl (mV)	CV (m/s)
normal value	Norm≥5	Norm≥5	Norm≥ 48	Norm≥5	Norm≥3	Norm≥ 40	Norm≥5	Norm≥5	Norm≥ 40
I/1	4.0	11.7	57	5.4	1.9	49	2.5	8.1	46
I/2	4.0	6.2	63	4.9	6.8	48	2.9	12	45
I/3	3.9	4.2	58	4.8	3.9	47	3.1	8.0	45
II/1	3.1	3.8	54	4.9	2.2	45	3.0	12	53
II/2	2.5	4.4	54	4.2	1.9	44	2.5	24	62
II/3	-	-	-	3.5	1.2	62	2.1	30	58
II/4	-	-	-	3.2	2.7	59	2.6	18	53

Ampl amplitude, *CV* conduction velocity, *DL* distal latency